Systematic study on visible light collimation by nanostructured slits in the metal surface*

Fu Jin-Xin(傅晋欣), Hua Yi-Lei(华一磊), Chen Yu-Hui(陈宇辉), Liu Rong-Juan(刘荣鹃), Li Jia-Fang(李家方), and Li Zhi-Yuan(李志远)†

Laboratory of Optical Physics, Institute of Physics, Chinese Academy of Sciences, Beijing 100190, *China*

(Received 28 September 2010; revised manuscript received 22 November 2010)

We present a systematic experimental investigation on visible light collimation by a nanostructured slit flanked with a pair of periodic array of grooves in gold thin film. A wide variety of aspects are considered, such as the polarization state, the transport path of incident light, the groove–groove spacing, the groove width and depth. Our results clearly show that the relationship between the collimation wavelength and the periodicity of the slit-groove structure accords well with the surface plasmon dispersion model proposed by previous researchers. Furthermore, the surface plasmon wave phase retardation effect induced by the surface structure is also verified via the measurement for samples with different groove widths and depths. These results indicate that the detailed geometry of the groove structure has obvious impacts on the collimation effect and the angular distribution of the diffraction light in the subwavelength plasmonic system.

Keywords: surface plasmon, collimation
PACS: 78.66.–W, 42.25.Fx, 42.79.Dj **DOI:** 10.1088/1674-1056/20/3/037806

1. Introduction

Plasmonics is currently attracting the attention of physicists for its various behaviours in nanostructure system and widespread potential applications.[1] When the light impinges on the surface of a metal, a collective oscillation of the electrons will be excited, which is named surface plasmon (SP) oscillation.[2] In 1998, Ebbesen *et al.*[3] found that this kind of surface wave could induce the extraordinary transmission in a periodic hole array in metal film with an optical thickness. Since then, tremendous attention has been paid to the studies of SP, such as extraordinary transmission (EOT),[4−12] surface-enhanced Raman scattering,[13−15] and energy conversion.[16−19] One of the marvelous progresses of the study plasmonics lies in the beaming effect of light in the nano-slit-groove system.[20−22] It breaks the conventional optical diffraction limits, and opens the door to the nano-optics. The SPs launched and scattered on the exit surface plays a key role in this beam collimation phenomenon. The grooves recollect the waves travelling along the surface, which are then scattered and constructively interfere in the near or far field zone and lead to a dramatically narrowed divergence of diffraction beam compared with that of a single-slit isotropic distribution. Many research groups focused on this interesting phenomenon and developed sorts of structures that have collimating effects to realize superhigh optical resolution,[23−25] shape the beams of edge-emitting semiconductor lasers.[26] Besides, the collimating effect in the microwave region is more obvious, which has been demonstrated by several groups both theoretically[27] and experimentally.[28,29]

So far, the collimating effect in visible region has been realized in a variety of occasions. Most of them consist of an air slit etched in the metal film with several hundred nanometers in width and tens of grooves in period surrounded on the lateral sides. The grooves are either etched in the metal layer itself or constructed in a dielectric superstrate on the metal.[30] Although a great deal of work has been done, the details of the collimating process are still not clear enough due to the lack of a systematic study on various collimating conditions with nanostructures of the same type. In this paper, we present a clear and thorough study on the collimating phenomenon of nano-slit-groove structure in metal film. By using a simple far-field angle-sensitive imaging setup, the polarization-, wavelength-, angle-, groove-spacing-, and groove-width-dependent collimating effects are visually observed in a single type of nano-slit-grooves. Importantly, this

*Project supported by the National Natural Science Foundation of China (Grant Nos. 60736041 and 10874238), and the National Key Basic Research Special Foundation of China (Grant No. 2007CB613205).
†Corresponding author. E-mail: lizy@aphy.iphy.ac.cn
© 2011 Chinese Physical Society and IOP Publishing Ltd

systematic study successfully has verified the phase retardation in two separate experiments, where the groove spacing and operating wavelength are varying, respectively.

The rest of the present paper is arranged as follows. In Section 2 we briefly describe how the plasmonic slit-groove samples are prepared and how their optical properties are measured. In Section 3 we present the detailed experimental data of beam collimation under a wide variety of geometric and physical parameters of the plasmonic system, and make comprehensive discussion to understand the observed phenomena. Finally in Section 4 we draw some conclusions from this study.

2. Sample preparation and characterization

The sample was made from a 300-nm-thick gold film deposited on a quartz substrate by a magnetron sputtering machine. Then we used the focused ion beam (FIB) milling method to directly write the pattern into the film. Figure 1(a) shows a typical scanning electron microscope (SEM) image of the cross section of our sample. The central slit is 300 nm deep and 100 nm wide while the lateral groove has the same width. However, the depth of the groove is hard to determine because the redeposit and crystallization effects during the FIB fabrication process can roughen the surface of the film. Therefore, we perform an additional atomic force micrroscope (AFM) scanning to characterize the surface topographies of the grooves and slits. Although our film is quite flat with a roughness level of 1 nm (root mean square value) before the FIB milling, the ion impinging and the crystallization of the gold atoms can seriously ruin the surface smoothness as shown in Figs. 1(b) and 1(c). Many gold grains with diameters in a range of 50–60 nm are produced by FIB etching. Fortunately the peak–valley distance in the roughened surface is within 15 nm, which is much smaller than the groove depth (typically 100 nm).

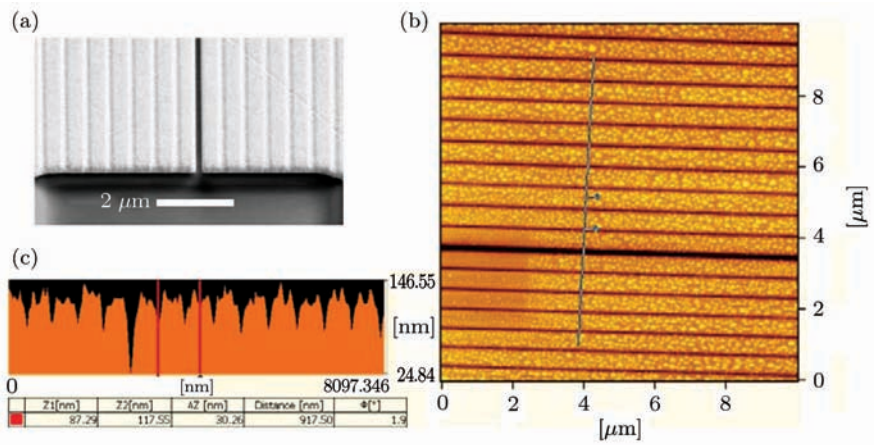


Fig. 1. (Colour online) (a) SEM image of the gold slit-groove structure etched by FIB. (b) AFM measurement of the surface topography of the sample. (c) The cross section profile of the blue line indicated in (b), where the two red lines correspond to the two arrows, one of which is positioned at the bottom of the groove.

The transmission light density distribution was recorded via a home-made angle-distribution measurement setup as shown in Fig. 2. A pre-collimated light beam illuminates on the sample from the left side. After travelling through the slit-groove structure, the dispersive light is then collected by a microscope objective lens, and finally reaches a CCD camera mounted at a parallel plane 15 cm away from the image spot. Since the pixel size of the CCD camera is as small as 7 μm, the angular resolution of our set can reach a level of 0.5 degree, which is accurate enough for this large dispersive system. We can simply derive the outgoing light beam angle θ_1 through the formula $\theta_1 = \arctan(v/u \cdot s/D)$, or just using the anti-tangential function to fit the $s-\theta_1$ curve. Here u and v are the object distance and the image distance respectively, D is the space between the image plane and the CCD camera, and s refers to the transverse span of the dispersive light in the CCD plane (typically on the order of tens of micrometers for the colli-

mation case). The surface waves scattered by the lateral structure interfere with each other and finally appear as an angular distribution at the far field, which is then recorded by the CCD camera. So it can be judged from the formula that the smaller the value of θ_1, which represents a narrower light divergence, the better the collimation of the beam by the sample.

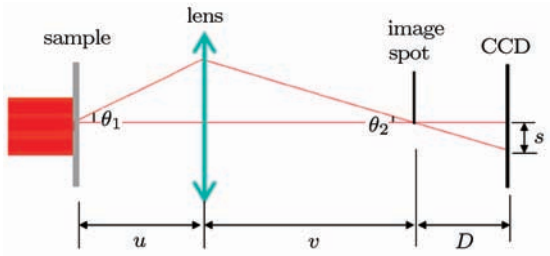


Fig. 2. (Colour online) Schematic of the light angle-distribution measurement setup. The maximum light dispersion angle that can be measured is determined by the numerical aperture of the objective lens. For a 10×(N.A. 0.3) lens the maximum value is about 18°, and for a 40×(N.A. 0.75) lens it is 48.5°.

3. Results and discussion

3.1. Effects of light polarization state and transport path

A white light source was first used to illuminate the samples with different periodicities ranging from 400 nm to 900 nm, as it is a broad band light source and can probe SP resonance at different periodicities and wavelengths simultaneously. We captured a series of images in various circumstances as seen in Fig. 3. Firstly, it is observed that the polarization of the light has a critical influence on the transmission through the structure. When the polarization direction is parallel to the slits, no surface plasmon is excited in the surface because TE polarization cannot be coupled to the SP wave, which possesses a TM character essentially. So there will be no dispersion when the light passes through neither from the air side nor from the glass side of the sample as shown in Figs. 3(a) and 3(b). When the light is vertically polarized to the slits and grooves (TM polarization), we obtain Fig. 3(c) for the air-side incidence and Fig. 3(d) for glass-side incidence. It is very interesting and also predictable that samples with different periodicities appear to display different colours in the screen [Fig. 3(c)], due to their special dispersions and different SP resonance wavelengths. There is an obvious angular chromatic dispersion in each column of Fig. 3(d), which does not happen in Fig. 3(c). This is reasonable because the resonance of the SP wave happens only in the groove surface.

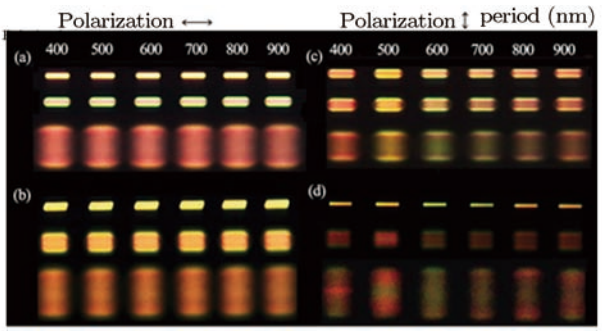


Fig. 3. (Colour online) Light intensity distribution images taken via CCD. In each panel, the six columns correspond to samples with different periodicities ranging from 400 nm to 900 nm. In each column, the three rows from top to bottom correspond to the images recorded as the screen gradually departs away from the image spot at 0 cm, 0.5 cm, and 2 cm, respectively. Images in panels (a) and (b) are measured with the parallel-polarized light incidence; images in panels (c) and (d) are taken in the vertical-polarized cases. On the other hand, images in panels (a) and (c) are taken with the light incident from air (air-side), while images in panels (b) and (d) are taken with the light incident from glass (glass-side).

When light first impinges on the air-groove interface, as in the Fig. 3(c) case, a collective oscillation of electrons in the structured gold surface is excited. The modes of the oscillation are dominated by the periodic grooves, where for some particular frequency a resonance effect along the corrugated metal surface is formed. In such a way, the light wave with the resonance wavelength will be strongly enhanced at the metal/air interface, which induces a better coupling between the surface plasmon polaritons (SPPs) on the two sides of the gold film and therefore a higher transmittance through the nano-slit when compared with those in the cases with operating wavelengths far from the resonance. However, on the outgoing side of the sample, there is only one slit where the transmitted wave diffracts into all directions, without any structural modulation, just as depicted by the images in Fig. 3(c). By comparison, we can see the scenario in Fig. 3(d) is quite different. In Fig. 3(d), the light first propagates through the structureless silt without frequency preferences, and then the diffracted waves which run along the surface will see the periodic structure in which case the SP resonance can be excited at a certain wavelength. Besides, the emergent light can be constructed in various angles for different wavelengths due to the specialized momentum matching condition. That is why we have different colours in

the central and lateral bands in Fig. 3(d). The observations in Fig. 3 clearly reflect the polarization, the frequency and the angle-dependent characteristics of the SP resonance induced by the periodic metallic nanostructure. This modulation of light propagation is useful for both collimation and dispersion device applications.

3.2. Effects of groove spacing

To obtain a more detailed study, we fabricated and characterized samples with smaller periodic intervals as shown in Fig. 4. Here we adopted the same measurement configuration as that in Fig. 3(d). It is very clear that for different periodicities, we have different colours in the central band, which represents the collimating area. When the periodicity is 660 nm, the blue light emerges near the 0 degree and the red light stays beside. With the decrease of the groove period, the angular spectrum presents a continuous shift. At first the red light converges to the centre, and reaches a narrowest line width at a periodicity of 570 nm with a maximum intensity. With the periodicity reducing, the red light beam diverges again and the central brightness decreases.

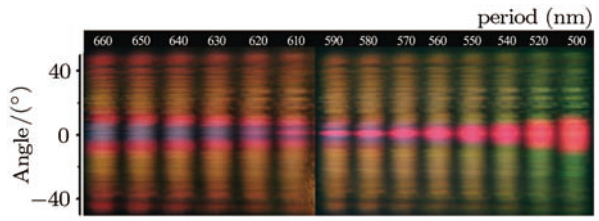


Fig. 4. (Colour online) Recorded CCD images showing collimating effects for different period slit-groove structures under white light illumination. The angle measurement spans between ±48°, which is limited to the numerical aperture of the objective lens.

To find out the exact relationship between the periodicity and the collimating wavelength more precisely, we changed the white light into a single-wavelength source. We used a He–Ne laser (632.8 nm) as the incident light and performed a similar measurement. The recorded angle distribution pictures are shown in Fig. 5. We can see that the 632.8 nm laser light is best collimated for the 570 nm (in periodicity) sample, in which the light intensity concentrates within the ±5° band around the centre. Although the line width of the central light band is narrower for the 580 nm and 590 nm cases than 570 nm, the 580 nm and 590 nm samples distribute more light to the wider angle area (larger than 5°). For the large-period structures (the left part of Fig. 5), the beams spread into all angles, which means that no beaming effect happens in all these configurations. We may pay attention to the special scenario where the 633 nm-period sample (which equals to the incident wavelength) does not collimate the light beam. Instead, there exists a black line in the centre.

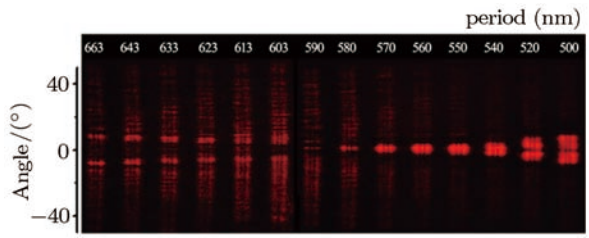


Fig. 5. (Colour online) Recorded light intensity distributions for different period slit-groove structures under He–Ne laser beam illumination at 632.8 nm.

In order to obtain the theoretical evidence for our experiments, we perform numerical simulations using the finite-difference time-domain (FDTD) method, which is widely used for the metallic nanostructure in the visible region. Figure 6 shows the calculated angle distribution of the relative light intensities for the aforementioned nanoslit samples. Apparently, the theoretical curves give the same conclusion as our experimental results in all the cases.

From previous studies,[3−5] we know that in the subwavelength scale metallic structure system, SP can be excited by external electromagnetic fields and then plays an important role in assisting light transmission through these metallic nanostructures. Generally, there is a frequency selective effect in this process due to the resonance of the SP wave. We might take it for granted that the light wave whose wavelength is the same as the structure period would satisfy the resonance condition and hence should be strongly enhanced. But unfortunately, all our experimental results indicate that the resonance enhancement happens at a longer wavelength. A relevant similar problem has raised a long-standing debate about the mechanism of the EOT during the past few years. The situation changed until 2008 when Liu and Lalanne[31] explicitly clarified the SP function in the EOT process. They pointed out that the resonance condition should be slightly modified as

$$\sqrt{\frac{\varepsilon_1\varepsilon_2}{\varepsilon_1+\varepsilon_2}}\frac{2\pi}{\lambda}+\frac{\arg(t)}{a_0}=m\cdot\frac{2\pi}{a_0}+k_0\sin\theta.$$

The most remarkable difference between this formula and the original one

$$\sqrt{\frac{\varepsilon_1\varepsilon_2}{\varepsilon_1+\varepsilon_2}}\frac{2\pi}{\lambda} = m\cdot\frac{2\pi}{a_0} + k_0\sin\theta$$

is the term $\arg(t)/a_0$, which is interpreted as the phase delay caused by the hole chain. When the SP wave propagates along the corrugated surface, it will experience a longer path than in a smooth interface. Then it can be deduced that the mismatch between the period and the transmission peak is due to the phase retardation of the SP wave. This mechanism also leads to the red-shift of the collimating wavelength compared with the periodicity as reflected in our experimental and theoretical results.

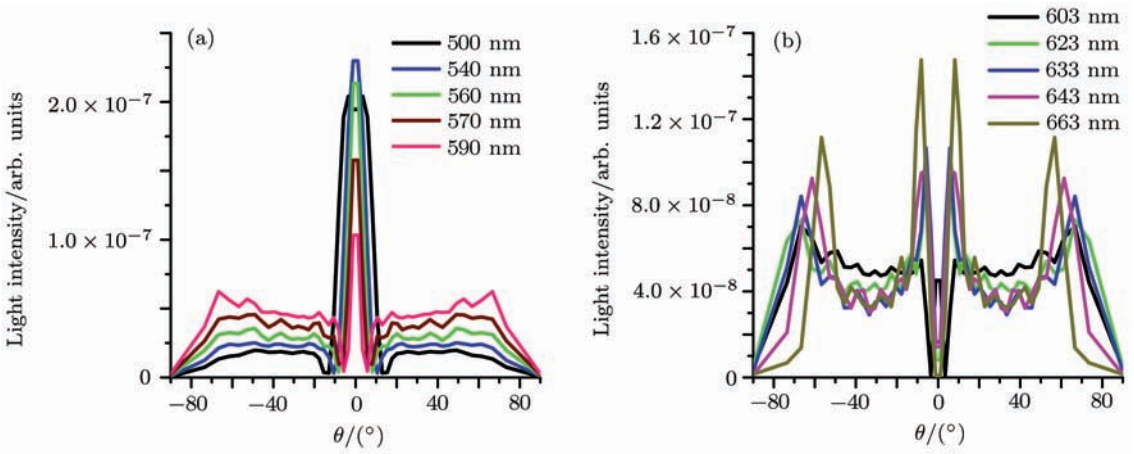


Fig. 6. (Colour online) Curves for calculated relative light intensity versus outgoing beam angle for different periods (marked in the bar). The incident wavelength is 632.8 nm. (a) Light beam gradually concentrates as the period changes from 500 nm to 570 nm; (b) When the period further grows, light disperses to larger angles and no beaming effect occurs, and the intensity decreases.

We performed another experiment to confirm this explanation. The 570 nm sample was picked out and the illumination light wavelengths ranging from 590 nm to 660 nm were separately selected via a monochrometer over the white light source. It can be clearly seen in Fig. 7 that the beam angle gradually decreases from the left to the right. The collimation condition is satisfied at the wavelengths 630 nm and 640 nm, which are close to the wavelength of the He–Ne laser. It should be pointed that the light distribution also seems to concentrate for the 650 nm case, which blurred the wavelength sensitivity in our beaming effects. We think, it is due to the wider line width (a span about 5nm) of the used white light (even after it passes through the monochrometer) than that of the laser light (less than 0.1 nm).

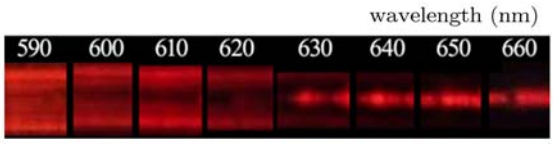


Fig. 7. (Colour online) Recorded light intensity distributions for the 570 nm structure under different incident light wavelengths (denoted by the superscripts).

3.3. Effects of groove width and depth

We continued our experiment with different groove widths and depths to verify the influence of the phase retardation, which will be reflected via the far field light intensity distribution. From Fig. 8, we can see that the depth change leads to a more obvious effect than the width change. We fabricated two groups of samples with the same spacing of 570 nm where the best collimation happens at 632.8 nm. In Fig. 8(a), the groove width is changed from 110 nm to 150 nm, and the beam spreads into a slightly larger angle when the grooves become wider. In Fig. 8(b), the groove depth is varied by decreasing the FIB milling time, and the central band of light becomes very dim for the shallower grooves. These results further support the phase retardation effect caused by the geometric details of the structure. The width and the depth both have an influence on the SP wave coupling between the two edges of the groove, which is essential to the phase delay for a single groove, and furthermore introduces the phase shift into the SPP resonance equation.



Fig. 8. (Colour online) Recorded light intensity distributions for samples with different widths (a) and depths (b) but the same period of 570 nm. The incident wavelength is 632.8 nm. (a) From left to right, the groove widths are 110 nm, 130 nm, and 150 nm, respectively; (b) From left to right, the groove depth decreases gradually.

4. Conclusions

In this paper, we have systematically studied the beam collimating effect of the subwavelength nanoslit-groove system in the visible light region experimentally and theoretically. We have built a series of nanoslit samples and set up a simple optical instrument to measure the dispersion, the diffraction, and the collimation features of white light and laser light. We have considered the influences from different geometric and physical aspects of the plasmonic nanosystem, which include the transport path and polarization state of the illumination light, the spacing, the depth, and the width of grooves. We have found that the excitation of SP wave in the exit plane of the nanoslit-groove structure by TM polarized light is indispensable to the observation of light beam collimation. Besides, the phase retardation plays a critical role in the SP resonance. Therefore, the groove width and depth have a great influence on SP propagation phase, and they determine the collimating condition for the periodic structures. Due to this phase retardation effect, the collimation wavelength is relatively red-shifted compared with the groove periodicity. Our research provides clarified experimental evidence for deeply understanding the SPP induced beam collimation phenomenon and constructing the corresponding physical picture. Our result is also helpful for exploring more detailed SPP resonance theory in corrugated metal surfaces. The experimental study can help to explore more potential applications in beam collimation, focusing, and other functionalities of plasmonic nanostrutures.

References

[1] Barnes W L, Dereux A and Ebbesen T W 2004 *Nature* **424** 824
[2] Maier S A 2007 *Plasmonics: Fundamentals and Applications* (Bath, UK: Springer)
[3] Ebbesen T W, Lezec H J, Ghaemi H F, Thio T and Wolff P A 1998 *Nature* **391** 667
[4] Kim T J, Thio T, Ebbesen T W, Grupp D E and Lezec H J 1999 *Opt. Lett.* **24** 256
[5] Martín-Moreno L, García-Vidal F J, Lezec H J, Pellerin K M, Thio T, Pendry J B and Ebbesen T W 2001 *Phys. Rev. Lett.* **86** 1114
[6] Barnes W L, Murray W A, Dintinger J, Devaux E and Ebbesen T W 2004 *Phys. Rev. Lett.* **92** 107401
[7] Fang X, Li Z Y, Long Y B, Wei H X, Liu R J, Ma J, Kamran M, Zhao H, Han X, Zhao B and Qiu X 2007 *Phys. Rev. Lett.* **99** 066805
[8] Sun M, Li Z Y, Cheng B Y, Zhang D Z, Yang H and Jin A 2007 *Phys. Lett.* A **365** 510
[9] Sun M, Liu R J, Li Z Y, Feng S, Cheng B Y, Zhang D Z, Yang H and Jin A 2006 *Phys. Rev.* B **74** 193404
[10] Ruan Z and Qiu M 2006 *Phys. Rev. Lett.* **96** 233901
[11] Hua Y L, Fu J X, Li J Y, Li Z Y and Yang H F 2010 *Chin. Phys.* B **19** 047309
[12] Gong Z Q and Liu J Q 2010 *Chin. Phys.* B **19** 067303
[13] Cobley C M, Rycenga M, Zhou F, Li Z Y and Xia Y 2009 *Angew. Chem. Int. Ed.* **48** 4824
[14] Lim B, Kobayashi H, Yu T, Wang J, Kim M J, Li Z Y, Rycenga M and Xia Y 2010 *J. Am. Chen. Soc.* **132** 2506
[15] Li Z Y and Xia Y 2010 *Nano Lett.* **10** 243
[16] Wang W, Wu S, Reinhardt K, Lu Y and Chen S 2010 *Nano Lett.* **10** 2012
[17] Sha W E I, Choy W C H and Chew W C 2010 *Opt. Express* **18** 5993
[18] Akimov Yu A, Ostrikov K and Li E. P 2009 *Plasmonics* **4** 107
[19] Okamoto K, Niki I, Shvartser A, Narukawa Y, Mukai T and Scherer A 2006 *JOSA* B **23** 1674
[20] Lezec H J, Degiron A, Devaux E, Linke R A, Martin-Moreno L, Garcia-Vidal F J and Ebbesen T W 2002 *Science* **297** 820
[21] Martín-Moreno L, García-Vidal F J, Lezec H J, Degiron A and Ebbesen T W 2003 *Phys. Rev. Lett.* **90** 167401
[22] García-Vidal F J, Lezec H J, Ebbesen T W and Martín-Moreno L 2003 *Phys. Rev. Lett.* **90** 213901
[23] Verslegers L, Catrysse P B, Yu Z, White J S, Barnard E S, Brongersma M L and Fan S 2009 *Nano Lett.* **9** 235
[24] Lin L, Goh X M, McGuinness L P and Roberts A 2010 *Nano Lett.* **10** 1936
[25] Srituravanich W, Pan L, Wang Y, Sun C, Bogy D B and Zhang X 2008 *Nat. Nanotechnology* **3** 733
[26] Yu N, Fan J, Wang Q, Pflügl C, Diehl L, Edamura T, Yamanishi M, Kan H and Capasso F 2008 *Nat. Photonics* **2** 564
[27] Hua L Y and Li Z Y 2009 *J. Appl. Phys.* **105** 013104
[28] Hibbins A P, Sambles J R and Lawrence C R 2002 *Appl. Phys. Lett.* **81** 4661
[29] Lockyear M J, Hibbins A P, Sambles J R and Lawrence C R 2004 *Appl. Phys. Lett.* **84** 2040
[30] Lin D Z, Chang C K, Chen Y C, Yang D L, Lin M W, Yeh J T, Liu J M, Kuan C H, Yeh C S and Lee C K 2006 *Opt. Express* **14** 3503
[31] Liu H and Lalanne P 2008 *Nature* **452** 728